

Short term bond shear stress and cracking control of reinforced self-compacting concrete one way slabs under flexural loading

Farhad Aslani^{*1}, Shami Nejadi² and Bijan Samali³

¹Centre for Infrastructure Engineering and Safety, School of Civil and Environmental Engineering, University of New South Wales, Australia

²School of Civil and Environmental Engineering, University of Technology Sydney, Australia

³Institute for Infrastructure Engineering, University of Western Sydney, Australia

(Received July 29, 2013, Revised February 4, 2014, Accepted May 22, 2014)

Abstract. Fibre-reinforced self-compacting concrete (FRSCC) is a high-performance building material that combines positive aspects of fresh properties of self-compacting concrete (SCC) with improved characteristics of hardened concrete as a result of fibre addition. To produce SCC, either the constituent materials or the corresponding mix proportions may notably differ from the conventional concrete (CC). These modifications besides enhance the concrete fresh properties affect the hardened properties of the concrete. Therefore, it is vital to investigate whether all the assumed hypotheses about CC are also valid for SCC structures. In the present paper, the experimental results of short-term flexural load tests on eight reinforced SCC and FRSCC specimens slabs are presented. For this purpose, four SCC mixes – two plain SCC, two steel, two polypropylene, and two hybrid FRSCC slab specimens – are considered in the test program. The tests are conducted to study the development of SCC and FRSCC flexural cracking under increasing short-term loads from first cracking through to flexural failure. The achieved experimental results give the SCC and FRSCC slabs bond shear stresses for short-term crack width calculation. Therefore, the adopted bond shear stress for each mix slab is presented in this study. Crack width, crack patterns, deflections at mid-span, steel strains and concrete surface strains at the steel levels were recorded at each load increment in the post-cracking range.

Keywords: fibre-reinforced self-compacting concrete; self-compacting concrete; crack control; flexural cracking; bond shear stress

1. Introduction

Self-compacting concrete (SCC) can be placed and compacted under its own weight with little or no vibration and without segregation or bleeding. SCC is used to facilitate and ensure proper filling and good structural performance of restricted areas and heavily reinforced structural members. It has gained significant importance in recent years because of its advantages (Aslani and Nejadi, 2012a,b,c). Recently, this concrete has gained wider use in many countries for different applications and structural configurations. SCC can also provide a better working

*Corresponding author, PhD, E-mail: F.Aslani@unsw.edu.au

environment by eliminating the vibration noise. Such concrete requires a high slump that can be achieved by superplasticizer addition to a concrete mix and special attention to the mix proportions. SCC often contains a large quantity of powder materials that are required to maintain sufficient yield value and viscosity of the fresh mix, thus reducing bleeding, segregation, and settlement. As the use of a large quantity of cement increases costs and results in higher temperatures, the use of mineral admixtures such as fly ash, blast furnace slag, or limestone filler could increase the slump of the concrete mix without increasing its cost (Aslani and Nejadi 2013a,b).

Fibre-reinforced self-compacting concrete (FRSCC) is a relatively recent composite material that combines the benefits of the SCC technology with the advantages of the fibre addition to a brittle cementitious matrix. It is a ductile material that in its fresh state flows into the interior of the formwork, filling it in a natural manner, passing through the obstacles, and flowing and consolidating under the action of its own weight. FRSCC can mitigate two opposing weaknesses: poor workability in Fibre-reinforced concrete (FRC) and cracking resistance in plain concrete (Aslani 2013; Aslani and Natoori 2013).

To control the crack width at the flexural member tension surface, designers can use the guidelines prescribed in various design codes. These guidelines are based on certain analytical solutions to crack width for conventional concrete (CC) that were developed by various researchers. There is no study about short term flexural cracking control of reinforced SCC and FRSCC one way slabs.

2. Research significance

2.1 Materials and mix proportions

In this study, the experimental results of short-term flexural load tests on eight reinforced SCC and FRSCC specimens slabs are presented. For this purpose, four SCC mixes – two plain SCC, two steel, two polypropylene, and two hybrid FRSCC slab specimens – are considered in the test program. In this study, all testing and measurement requirements are based on the Nejadi (2005) research study and we aimed to compare SCC and FRSCC slab series experimental results with CC (Nejadi 2005) slab series experimental results. The tests were conducted to study the development of SCC and FRSCC flexural cracking under increasing short-term loads from first cracking through to flexural failure. Crack width, crack patterns, deflections at mid-span, steel strains and concrete surface strains at the steel levels were recorded at each load increment in the post-cracking range.

The major objectives of the experimental program were:

(a) To gain a better understanding of the mechanisms associated with SCC and FRSCC flexural cracking of slab, and the influence of those factors that affect the spacing and width of flexural cracks under short-term loading.

(b) To obtain bond shear stresses for SCC and FRSCC slabs crack width calculation.

3. Experimental Study

3.1 Materials

In this experimental study, shrinkage limited cement (SLC) corresponding to the ASTM C183-08 (2000) (AS 3972 2010) standard was used. SLC is manufactured from specially prepared portland cement clinker and gypsum. It may contain up to 5% of AS 3972 approved additions. The

chemical, physical, and mechanical properties of the cement used in the experiments are shown in Table 1. The chemical, physical, and mechanical properties adhere to the limiting value or permissible limits specified in AS 2350.2, 3, 4, 5, 8, and 11 (2006).

Table 1 Properties of cement, fly ash, and ground granulated blast furnace slag (GGBFS)

Cement		Fly ash		GGBFS	
Chemical properties		Chemical properties		Chemical properties	
CaO	64.5%	Al ₂ O ₃	26.40%	Al ₂ O ₃	14.30%
SiO ₂	19.3%	CaO	2.40%	Fe ₂ O ₃	1.20%
Al ₂ O ₃	5.2%	Fe ₂ O ₃	3.20%	MgO	5.40%
Fe ₂ O ₃	2.9%	K ₂ O	1.55%	Mn ₂ O ₃	1.50%
MgO	1.1%	MgO	0.60%	SO ₃	0.20%
SO ₃	2.9%	Mn ₂ O ₃	< 0.1%	Cl	0.01%
K ₂ O	0.56%	Na ₂ O	0.47%	Insoluble Residue	0.50%
Na ₂ O	<0.01%	P ₂ O ₅	0.20%	LOI	-1.10%
Cl	0.02%	SiO ₂	61.40%	Physical properties	
LOI	2.8%	SO ₃	0.20%	Fineness Index	435 m ² /kg
Physical properties		SrO	< 0.1%		
Autoclave expansion	TiO ₂	TiO ₂	1.00%		
Fineness index	405 m ² /kg	Physical properties			
Mechanical properties		Moisture	< 0.1%		
Initial setting time	90 mins	Fineness 45 micron	78% passed		
Final setting time	135 mins	Loss on ignition	2.30%		
Soundness	1.0 mm	Sulfuric anhydride	0.20%		
Drying shrinkage	590 μ strain	Alkali content	0.50 %		
f'_c (3 Days)	37.2 MPa	Chloride ion	< 0.001%		
f'_c (7 Days)	47.3 MPa	Relative density	2.02 %		
f'_c (28 Days)	60.8 MPa	Relative water requirement	97%		
		Relative strength 28 days	88%		

Table 2 Properties of crushed latite volcanic rock coarse aggregate, Nepean river gravel fine aggregate, and Kurnell natural river sand fine aggregate

Crushed latite volcanic rock coarse aggregate		Nepean river gravel fine aggregate		Kurnell natural river sand fine aggregate	
Characteristics	Results	Characteristics	Results	Characteristics	Results
Sieve size	Passing (%)	Sieve size	Passing (%)	Sieve size	Passing (%)
13.2 mm	100	6.7 mm	100	1.18 mm	100
9.5 mm	89	4.75 mm	99	600 micron	98
6.7 mm	40	2.36 mm	83	425 micron	87
4.75 mm	7	1.18 mm	64	300 micron	46

Table 2 Continued

2.36 mm	1	600 micron	42	150 micron	1
1.18 mm	1	425 micron	28	Material finer than 75 micron	Nil
Material finer than 75 micron (%)	1	300 micron	19	Uncompacted bulk density (t/m^3)	1.39
Mis-shapen particles (%)		150 micron	8	Compacted bulk Density (t/m^3)	1.54
Ratio 2:1	13	Material finer than 75 micron (%)	3	Particle density (Dry) (t/m^3)	2.58
Ratio 3:1	1	Uncompacted bulk Density (t/m^3)	1.52	Particle density (SSD) (t/m^3)	2.59
Flakiness index (%)	20	Compacted bulk density (t/m^3)	1.64	Apparent particle density (t/m^3)	2.62
Uncompacted bulk density (t/m^3)	1.36	Particle density (Dry) (t/m^3)	2.58	Water absorption (%)	0.6
Compacted bulk density t/m^3	1.54	Particle density (SSD) (t/m^3)	2.60	Silt content (%)	4
Moisture condition of the aggregate (%)	1.3	Apparent particle density (t/m^3)	2.63		
Particle density (Dry) (t/m^3)	2.65	Water absorption (%)	0.7		
Particle density (SSD) (t/m^3)	2.70	Silt content (%)	7		
Apparent particle density (t/m^3)	2.79	Degradation factor of fine aggregate	90		
Water absorption (%)	1.9	Moisture content (%)	5.5		
Ave. dry strength (kN)	391	Method of determining voids content			
Ave. wet strength (kN)	293	% Voids	41.7		
Wet/dry strength variation (%)	25	The mean flow time (Sec.)	26.5		
Test fraction (mm)	-9.5+6.7				
The amount of significant breakdown (%)	<0.2				
Los angeles value grd. 'K' (%Loss)	13				

Table 3 The physical and mechanical properties of fibres

Fibre type	Fibre name	Density (kg/m^3)	Length (l)	Diameter (d)	Aspect ratio (l/d)	Tensile strength (MPa)	Modulus of elasticity (GPa)	Cross-section form	Surface structure
Steel	Dramix RC-80/60-BN	7850	60	0.75	80.0	1050	200	Circular	Hooked end
Polipropylene (PP)	Synmix 65	905	65	0.85	76.5	250	3	Square	Rough

Table 4 The proportions of the concrete mixtures (based on SSD condition)

Constituents	N-SCC	D-SCC	S-SCC	DS-SCC
Cement (kg/m ³)	160	160	160	160
Fly Ash (kg/m ³)	130	130	130	130
GGBFS (kg/m ³)	110	110	110	110
Cementitious content (kg/m ³)	400	400	400	400
Water (lit/m ³)	208	208	208	208
Water cementitious ratio	0.52	0.52	0.52	0.52
Fine aggregate (kg/m ³)				
Coarse sand	660	660	660	660
Fine sand	221	221	221	221
Coarse aggregate (kg/m ³)	820	820	820	820
Admixtures (lit/m ³)				
Superplasticiser	4	4.86	4.73	4.5
VMA	1.3	1.3	1.3	1.3
High range water reducing agent	1.6	1.6	1.6	1.6
Fibre content (kg/m ³)				
Steel	-	30	-	15
PP	-	-	5	3

3.1.2 Fly ash

It is important to increase the amount of paste in SCC because fly ash is an agent to carry the aggregates. Eraring fly ash (EFA) is a natural pozzolan. It is a fine cream/grey powder that is low in lime content. The chemical and physical properties of EFA used in the experimental study are given in Table 1. The chemical, physical, and mechanical properties of the EFA used adhere to the limiting value or permissible limits specified in ASTM C311-11b (2000) (ACI 232.2R-03, 2004; AS 2350.2, 2006; AS 3583.1, 2, 3, 5, 6, 12, and 13, 1998).

3.1.3 Ground granulated blast furnace slag

Granulated blast furnace slag (GGBFS) is another supplementary cementitious material that is used in combination with SLC. GGBFS used in the experiment originated in Boral, Sydney, and it conformed to ASTM C989-06 (2000) (ACI 233R-95, 2000; and AS 3582.2, 2001) specifications. The chemical and physical properties of GGBFS are given in Table 1.

3.1.4 Aggregate

In this study, crushed volcanic rock (i.e., latite) coarse aggregate was used with a maximum aggregate size of 10 mm. Nepean river gravel with a maximum size of 5 mm and Kurnell natural river sand fine aggregates were also used. The sampling and testing of aggregates were carried out in accordance with ASTM C1077-13 (2000) (AS 1141, 2011; RTA, 2006) and the results for coarse and fine aggregates are shown in Tables 2, respectively.

3.1.5 Admixtures

The superplasticiser, viscosity-modifying admixture, and high-range water-reducing agent were used in this study. The new superplasticiser generation Glenium 27 complies with AS 1478.1 (2000) type High Range Water Reducer (HRWR) and ASTM C494 (2000) types A and F are used.

The Rheomac VMA 362 viscosity modifying admixture that used in this study is a ready-to-use, liquid admixture that is specially developed for producing concrete with enhanced viscosity and controlled rheological properties. Pozzolith 80 was used as a high-range water-reducing agent in the mixes. It meets AS 1478 (2000) Type WRRe, requirements for admixtures.

3.1.6 Fibres

In this study, two commercially available fibres, Dramix RC-80/60-BN type steel fibres and Synmix 65 type polypropylene (PP) fibres, were used. The mechanical, elastic and surface structure properties of the steel and PP fibres are summarized in Table 3.

3.2 Mixture proportions

One control SCC mixture (N-SCC) and three fibre-reinforced SCC mixtures were used in this study. Fibre-reinforced SCC mixtures contain steel (D-SCC), PP (S-SCC), and hybrid (steel + PP) (DS-SCC) fibres. The content proportions of these mixtures are given in Table 4. These contents were chosen to attempt to keep compressive strength to a level applicable to construction. As shown in Table 4, cement, fly ash, GGBFS, water, fine and coarse aggregates, VMA, and high range water reducing agent constituents amount are same for four mixes. But, fibre amount and superplasticiser that are used in the mixes are different.

A forced pan type of mixer with a maximum capacity of 150 liters was used. The volume of a batch with fibres was kept constant at 50 liters. First, powders and sand are mixed for 10 s and water and superplasticiser are added and mixed for 110 s and the coarse aggregate is added and at the end fibres are added to the pan and mixed for 90 s.

3.3 Mechanical properties samples' preparation and curing conditions

We used six 150 mm × 300 mm cylindrical moulds for the determination of compressive and splitting tensile strengths per each age, and three cylindrical moulds 150 mm × 300 mm are used for the determination of the modulus of elasticity per each age. Meanwhile, three 100 mm × 100 mm × 350 mm beam moulds are used for the determination of modulus of rupture per each age. Specimens for testing the hardened properties are prepared by direct pouring of concrete into moulds without compaction. The specimens are kept covered in a controlled chamber at $20 \pm 2^\circ\text{C}$ for 24 h until demoulding. Thereafter, the specimens are placed in water presaturated with lime at 20°C . These compressive and tensile strengths, modulus of elasticity and modulus of rupture specimens are tested at 3, 7, 14, 28, 56, and 91 days. For each test, separated specimens are used and surface of specimens are smoothed.

3.4 Mechanical properties samples' test methods

The compressive strength test, performed on 150 mm × 300 mm cylinders, followed AS 1012.14 (1991) and ASTM C39 (2000) tests for compressive strength of cylindrical concrete specimens. The cylinders were loaded in a testing machine under load control at the rate of 0.3 MPa/s until failure. The splitting tensile test, run on 150 mm × 300 mm cylinders, was in accordance with the AS 1012.10 (2000) and ASTM C496 (2000) tests for splitting tensile strength

of cylindrical concrete specimens, although ACI committee 544.2R (1999) hardly recommends the use of the test on fibre-reinforced concrete. The running arose because the ratio of fibre length to cylinder diameter took a low value of 0.23 in the work and because some investigators have shown that the ASTM C496 test is applicable to fibre-reinforced concrete specimens.

The modulus of elasticity test that followed the AS 1012.17 (1997) and ASTM C469 was done to 150 mm × 300 mm cylinders. The flexural strength (modulus of rupture, MOR) test, conducted using 100 mm × 100 mm × 350 mm test beams under third-point loading, followed the AS 1012.11 (2000) and ASTM C1018 (2000) test for flexural toughness and first-crack strength of fibre-reinforced concrete. The mid-span deflection was the average of the ones detected by the transducers through contact with brackets attached to the beam specimen.

3.5 Properties of fresh concrete

The experiments required for the SCC are generally carried out worldwide under laboratory conditions. These experiments test the liquidity, segregation, placement, and compacting of fresh concrete. Conventional workability experiments are not sufficient for the evaluation of SCC. Some of the experiment methods developed to measure the liquidity, segregation, placement, and compaction of SCC are defined in the European guidelines (2005) and ACI 237R-07 (2007) for SCC, including specification, production and use as slump–flow, V-funnel, U-box, L-box and fill-box tests.

This study performed slump flow, $T_{50\text{cm}}$ time, J-ring flow, V-funnel flow time, and L-box blocking ratio tests. In order to reduce the effect of loss of workability on the variability of test results, the fresh properties of the mixes were determined within 30 min after mixing. The order of testing is as follows: 1. Slump flow test and measurement of $T_{50\text{cm}}$ time; 2. J-ring flow test, measurement of difference in height of concrete inside and outside the J-ring and measurement of $T_{50\text{cm}}$ time; 3. V-funnel flow tests at 10 s $T_{10\text{s}}$ and 5 min $T_{5\text{min}}$; and 4. L-box test.

3.6 Slab specimens preparation and test set up

Eight singly reinforced SCC and FRSCC slab specimens were cast and moist cured for 28 days. All the specimens were simply supported on a 3500 mm span and tested to failure to investigate the distribution and extent of primary and secondary cracking under short-term loading using two equal point loads applied at the third points on the span, at ages greater than 28 days. Crack widths were monitored on the side face of the specimens from initial cracking up to a load sufficient to cause the tensile steel to yield. The schematic diagram of the test set-up is shown in Fig. 1. Deflections at mid-span, crack widths, crack patterns, steel strains within the high moment region, and concrete surface strains at the steel level were recorded at each load increment in the post-cracking range and development of the primary crack pattern was monitored throughout the test. The parameter is varied in the tests, including the four SCC mixes – plain SCC, steel, polypropylene, and hybrid FRSCC. Details of the slab specimens are given in Table 5. Two identical specimen “a” and “b” were constructed for each SCC mix.

The slab specimens were each nominally 3500 mm long by 400 mm wide. In all slabs the nominal distance from the soffit to the centroid of the main reinforcement was 25 mm. Slabs series were each reinforced with 4N12. Details of the cross-sections and reinforcement layouts for slab specimens are shown in Fig. 2.

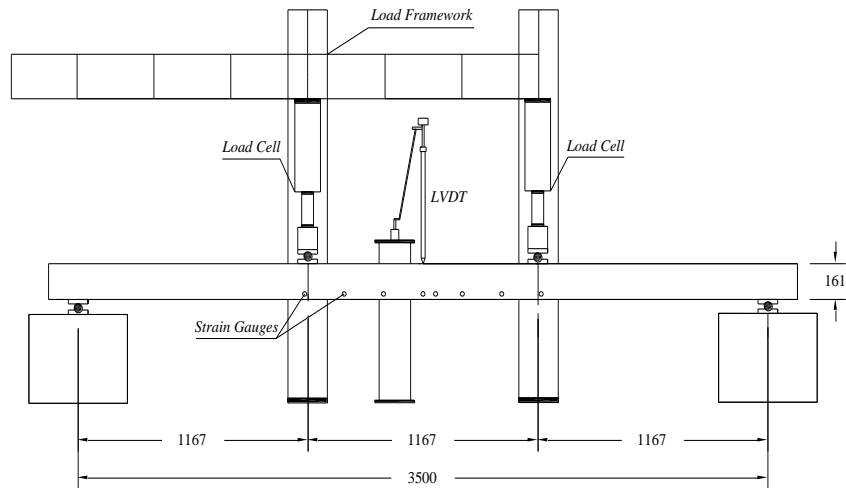


Fig. 1 Test arrangement for all specimens

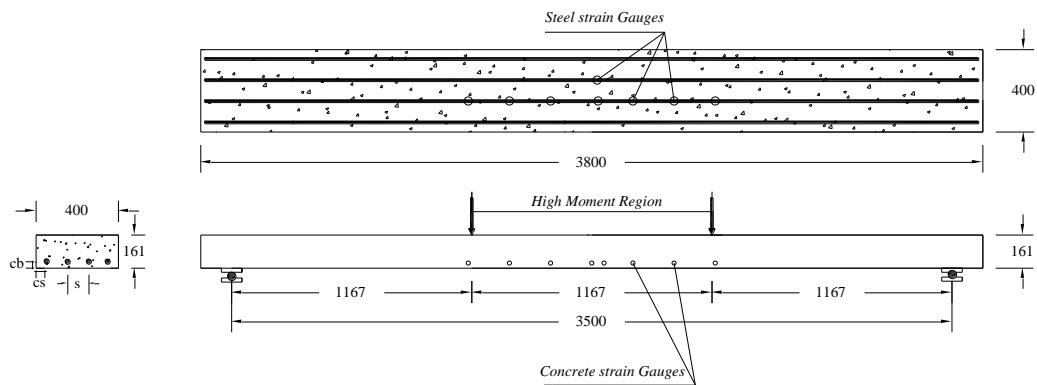


Fig. 2 Dimensions and reinforcement details for slab specimens

All specimens were constructed in 3800 mm long formwork and were simply supported over a 3500 mm span. Eight electric resistance concrete strain gauges (60 mm) targets were glued on the side face of each specimen at the steel level to measure the concrete surface strains and eight electric resistance steel strain gauges (5 mm) targets were glued on middle rebar in the slab specimens for measuring the steel strains in the high moment region (as shown in Fig. 2). A microscope with a magnification factor of 50 was used to measure the crack widths. Deflection at mid-span was measured using a MTS-Temposonics R-Series position sensor. The position sensor and resistance strain gauge measurements were retrieved through a data acquisition system connected to a computer, while load was supplied by a hydraulic jack connected to an electrically powered pressure pump. Before casting each specimen, the inside surface of the mould was cleaned and coated with a thin layer of concrete release agent to prevent adhesion of the concrete.

The SCC was placed into the mould in equal layers until each surface layer became smooth. Sufficient concrete was placed into the top layer to overfill the mould, after which the surface was stripped off and finished with a steel trowel. The companion specimens were also cast at the same time as the test specimens. Within two hours of casting the specimens were covered with wet hessian and plastic sheets and left in their moulds for 3 days. After 3 days they were removed and kept moist continuously by a thick covering of wet hessian. After 28 days the wet hessian was removed and the specimens were identified and tested at different ages. Each specimen was slowly and gradually loaded to failure over a period of approximately four hours. Fig. 3 shows views of the experimental set-up. Each specimen was simply supported at each end before testing, and then one Temposonics R-Series position sensor was attached at the mid-span and linked to a computer. Electric resistance concrete strain gauges targets were glued to the concrete surface and initial strain measurements were recorded (see Fig. 3).



Fig. 3 General view of loading cells, concrete strain gauges, and position sensor test set-up

Table 6 The SCC mixes workability characteristics

Workability characteristics	N-SCC	D-SCC	S-SCC	DS-SCC
Average spreading diameter (mm)	680	670	700	650
Flow time T _{50cm} (s)	2.7	3.8	2.5	3.2
Average J-Ring diameter (mm)	655	580	570	560
Flow time T _{50cm} J-Ring (s)	3.2	5	6	5
L-box test	0.87	Blocked*	Blocked	Blocked
Flow time V-funnel (s)	6	7	Blocked	Blocked
V-funnel at T _{5minutes} (s)	4	5	Blocked	Blocked
Entrapped air (%)	1.3	1.2	1.2	1.0
Specific gravity (kg/m ³)	2340	2274	2330	2385

* Fibres are the main reason for blockage.

Table 7 Compressive strength, tensile strength, modulus of elasticity, and modulus of rupture of SCC mixtures at different ages

Compressive strength (MPa)					Tensile strength (MPa)				
Age (days)	N-SCC	D-SCC	S-SCC	DS-SCC	Age (days)	N-SCC	D-SCC	S-SCC	DS-SCC
3	12.45	18.50	13.65	14.30	3	1.65	2.32	1.16	1.76
7	21.80	25.30	22.50	26.30	7	2.26	3.38	1.93	2.51
14	29.05	34.30	32.45	38.10	14	2.80	3.87	3.05	3.54
28	33.30	38.00	38.10	45.00	28	3.60	4.54	3.56	4.09
56	40.60	50.50	42.90	50.75	56	4.17	5.35	4.02	4.33
91	46.40	51.15	47.65	52.00	91	4.57	5.44	4.41	4.80
Modulus of elasticity (GPa)					Modulus of rupture (MPa)				
Age (days)	N-SCC	D-SCC	S-SCC	DS-SCC	Age (days)	N-SCC	D-SCC	S-SCC	DS-SCC
3	25.23	24.45	25.36	26.78	3	2.50	3.35	3.13	2.47
7	27.84	26.57	27.87	30.13	7	3.35	4.10	4.26	3.81
14	32.24	29.14	29.68	31.26	14	4.66	5.40	4.60	4.80
28	35.39	35.76	35.76	36.10	28	5.00	6.37	5.00	5.40
56	35.58	36.44	36.32	37.03	56	5.87	6.72	6.50	6.52
91	37.79	37.58	37.47	38.12	91	7.13	7.23	6.76	7.21

4. Experimental results

4.1 Properties of fresh concrete

The results of various fresh properties tested by the slump flow test (slump flow diameter and $T_{50\text{cm}}$); J-ring test (flow diameter); L-box test (time taken to reach 400 mm distance $T_{400\text{mm}}$, time taken to reach 600 mm distance $T_{600\text{mm}}$, time taken to reach 800 mm distance T_L , and ratio of heights at the two edges of L-box [H_2/H_1]); V-funnel test (time taken by concrete to flow through V-funnel after 10 s $T_{10\text{s}}$); the amount of entrapped air; and the specific gravity of mixes are given in Table 6. The slump flow test judges the capability of concrete to deform under its own weight against the friction of the surface with no restraint present. A slump flow value ranging from 500 to 700 mm for self-compacting concrete was suggested (European guidelines, 2005). At a slump flow > 700 mm the concrete might segregate, and at < 500 mm, the concrete might have insufficient flow to pass through highly congested reinforcements. All the mixes in the present study conform to the above range, because the slump flow of SCC is in the range of 600–700 mm. The slump flow time for the concrete to reach a diameter of 500 mm for all mixes was less than 4.5 s. The J-ring diameters were in the range of 560–655 mm. In addition to the slump flow test, a V-funnel test was also performed to assess the flow ability and stability of SCC. V-funnel flow time is the elapsed time in seconds between the opening of the bottom outlet, depending when it is opened ($T_{10\text{s}}$ and $T_{5\text{min}}$), and the time when light becomes visible at the bottom when observed from the top.

According to the European guidelines (2005), a period ranging from 6 to 12 s is considered

adequate for SCC. The V-funnel flow times in the experiment were in the range of 7-11 s. The test results of this investigation indicated that all mixes met the requirements of allowable flow time. About V-funnel flow time test results for the N-SCC mix was 6 s and for the D-SCC was 7 s and for other fibre reinforced SCC mixes are blocked, obviously. The maximum size of coarse aggregate was restricted to 10 mm to avoid a blocking effect in the L-box for N-SCC mix. The gap between rebars in the L-box test was 35 mm. The L-box ratio H_2/H_1 for the N-SCC mix was above 0.8 which is, according to the European guidelines and, obviously, for other mixes is blocked. A total spread over 700 mm was measured and no sign of segregation or considerable bleeding in any of the mixtures was detected as the mixtures showed good homogeneity and cohesion.

4.2 Compressive and tensile strengths, modulus of elasticity, and modulus of rupture

Table 7 presents the compressive and tensile strengths, modulus of elasticity, and modulus of rupture of the N-SCC, D-SCC, S-SCC, and DS-SCC mixes achieved at different ages. Compressive strength samples with fibre mixes are higher than N-SCC mix. The results indicate that the compressive strength of the DS-SCC mix at 91 days is 11%, 1%, and 8% higher than the N-SCC, D-SCC, and S-SCC mixes, respectively. Moreover, the results indicate that the tensile strength of the D-SCC mix at 91 days is 16%, 19%, and 12% higher than that of the N-SCC, S-SCC, and DS-SCC mixes, respectively. Additionally, the results indicate that the tensile strength of the DS-SCC mix at 91 days is 0.8%, 1%, and 1% higher than that of the N-SCC, D-SCC, and S-SCC mixes, respectively. Also, the results indicate that modulus of rupture of D-SCC mix at 91 days is 1%, 6%, and 0.2% higher than that of the N-SCC, S-SCC, and DS-SCC mixes, respectively.

4.3 Short term flexural cracking control test result of slabs

4.3.1 N-SCC slab series

Slabs N-SCC-a and N-SCC-b containing the 4N12 longitudinal tensile reinforcing bars, with 25 mm clear bottom cover were tested at ages 62 and 63 days respectively. Cracking first occurred approximately at load of $P = 8$ kN in both N-SCC-a and N-SCC-b. The number of cracks increased as the applied load increased and at approximately 70% of the ultimate load, 14 cracks were located inside the high moment region (H.M.R) for N-SCC-a, and 13 cracks for N-SCC-b respectively. The measured final average crack spacings at this load stage were 95 mm for N-SCC-a and 94 mm for N-SCC-b. The ratio of maximum crack width to average crack width at load stage $P = 26$ kN was 1.29 for N-SCC-a and 1.17 for N-SCC-b. The measured maximum and average crack widths within the high moment region at the bottom fibre of the slabs versus applied load are illustrated in Fig. 4.

The measured mid-span deflections of slabs N-SCC-a and N-SCC-b are plotted against load in Fig. 5, respectively. As shown, slab series N-SCC illustrated good ductile behaviour with an extended flat plateau in the load-deflection curve. The ultimate strength was reached when $P = 49$ kN for N-SCC-a and $P = 48.5$ kN for N-SCC-b when crushing the top compressive fibre occurred and corresponding deflections were 180 mm and 163 mm. Slab series N-SCC failed in flexure in the pure moment zone, with the compressive concrete crushing above a crack (see Fig. 6).

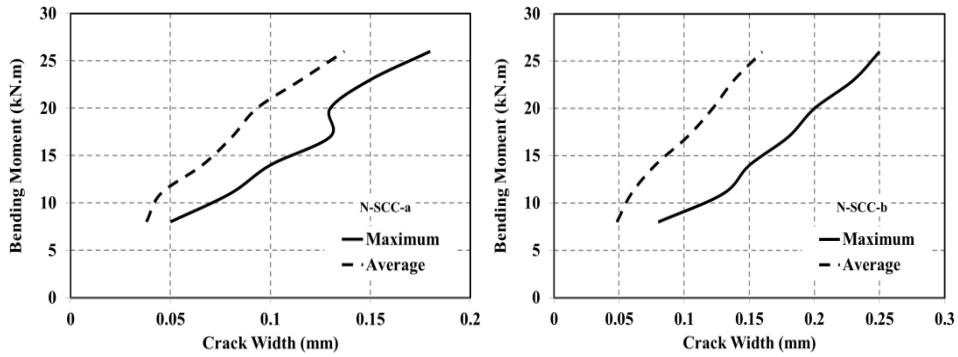


Fig. 4 Crack width vs. applied bending moment for slabs N-SCC-a and N-SCC-b

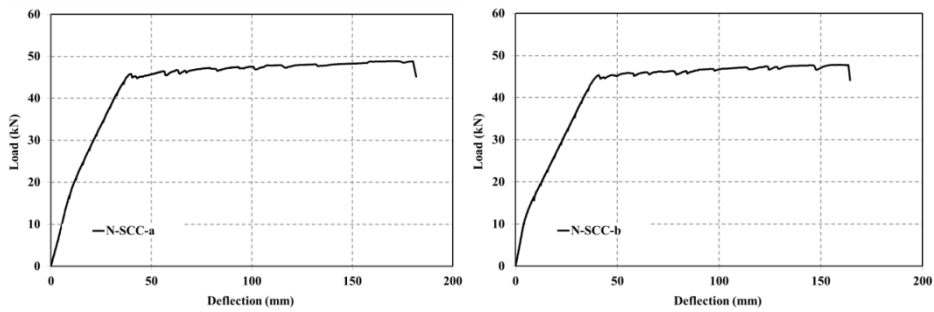


Fig. 5 Load-deflection curve for slabs N-SCC-a and N-SCC-b at mid-span



Fig. 6 General view of slab N-SCC-a failure

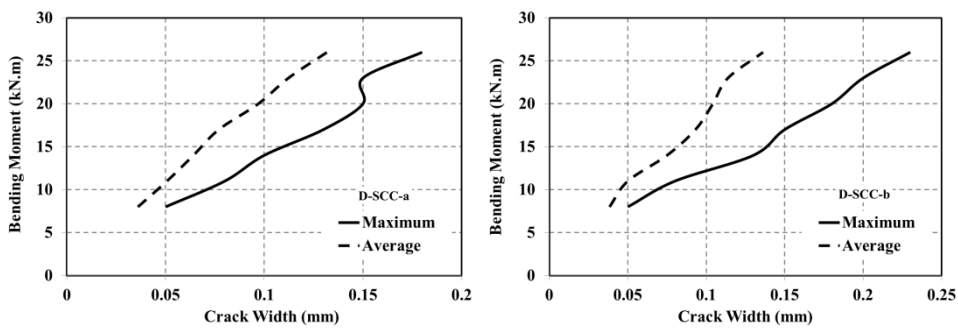


Fig. 7 Crack width vs. applied bending moment for slabs D-SCC-a and D-SCC-b

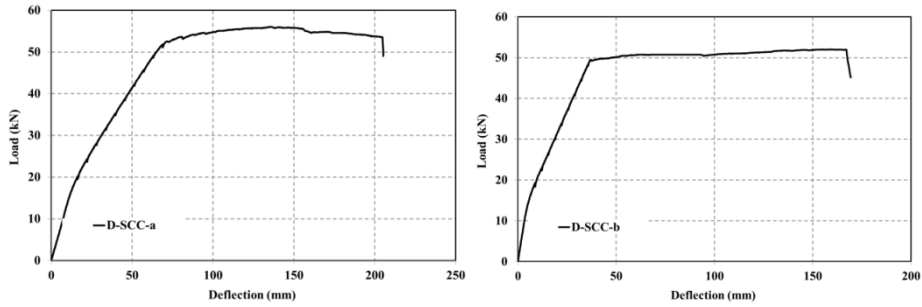


Fig. 8 Load-deflection curve for slabs D-SCC-a and D-SCC-b at mid-span

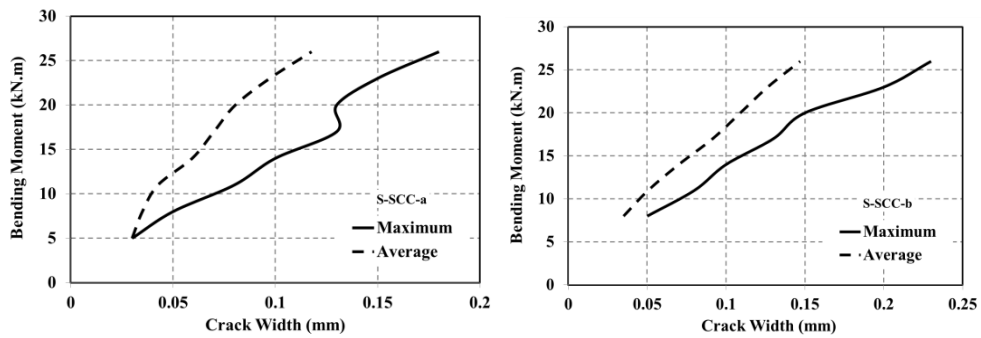


Fig. 9 Crack width vs. applied bending moment for slabs S-SCC-a and S-SCC-b

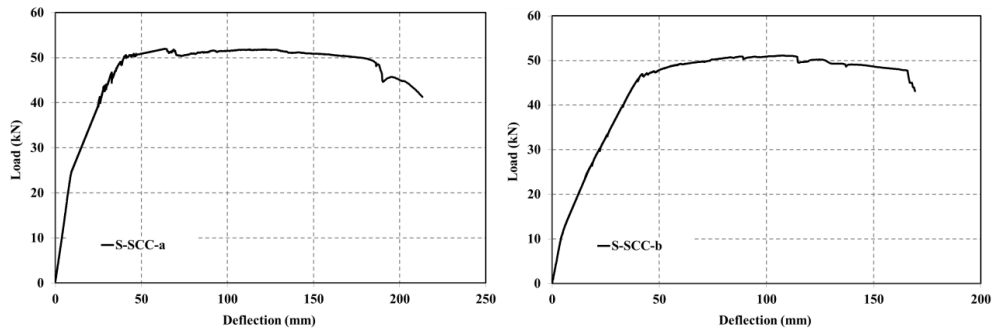


Fig. 10 Load-deflection curve for slabs S-SCC-a and S-SCC-b at mid-span

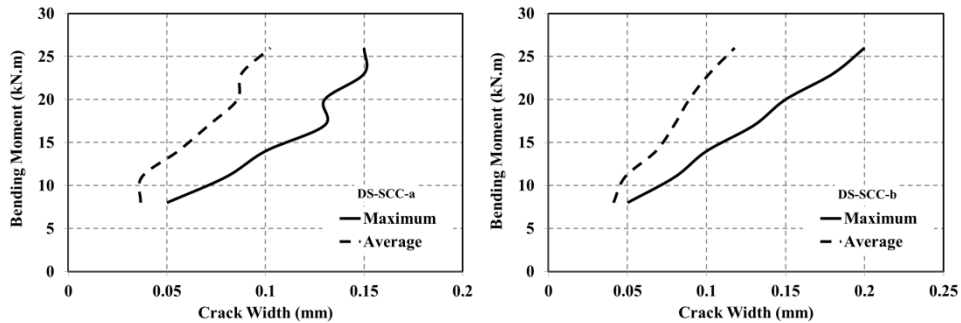


Fig. 11 Crack width vs. applied bending moment for slabs DS-SCC-a and DS-SCC-b

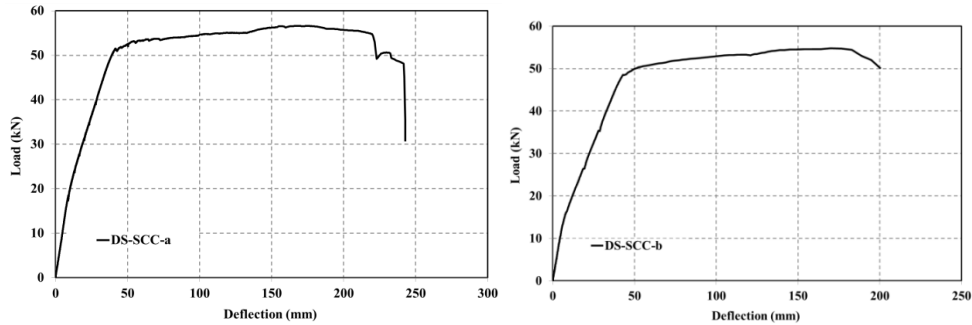


Fig. 12 Load-deflection curve for slabs DS-SCC-a and DS-SCC-b at mid-span

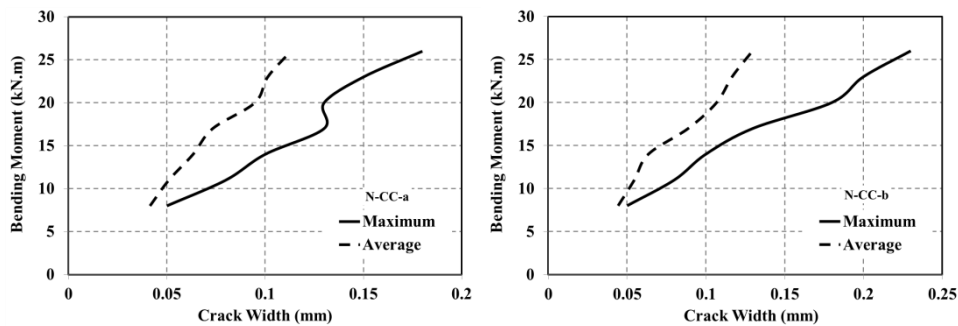


Fig. 13 Crack width vs. applied bending moment for slabs N-CC-a and N-CC-b (Nejadi 2005)

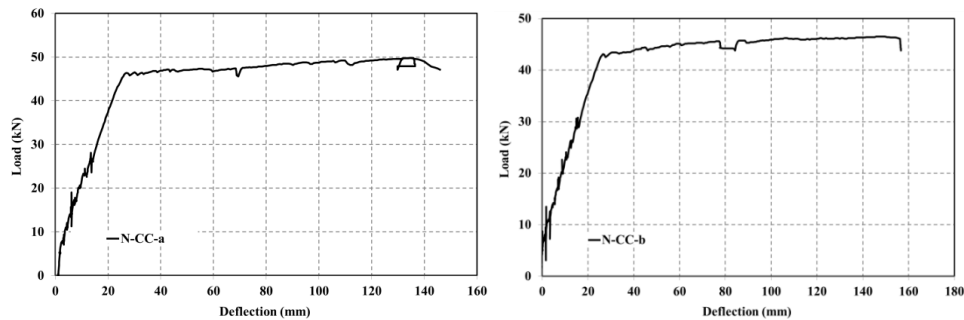


Fig. 14 Load-deflection curve for slabs N-CC-a and N-CC-b at mid-span (Nejadi 2005)

4.3.2 D-SCC slab series

Slabs D-SCC-a and D-SCC-b containing the 4N12 longitudinal tensile reinforcing bars and steel fibres, with 25 mm clear bottom cover were tested at ages 65 and 66 days respectively. Cracking first occurred approximately at load of $P = 8$ kN in both D-SCC-a and D-SCC-b same as N-SCC series. The number of cracks increased as the applied load increased and at approximately 70% of the ultimate load, 11 cracks were located inside the high moment region (H.M.R) for D-SCC-a, and 13 cracks for D-SCC-b respectively. The measured final average crack spacings at this load stage were 106 mm for D-SCC-a and 96 mm for D-SCC-b. The ratio of maximum crack width to average crack width at load stage $P = 26$ kN was 1.10 for D-SCC-a and 1.33 for D-SCC-b. The measured maximum and average crack widths within the high moment region at the bottom

fibre of the slabs versus applied load are illustrated in Fig. 7.

The measured mid-span deflections of slabs D-SCC-a and D-SCC-b are plotted against load in Fig. 8, respectively. Maximum deflection at failure loading of D-SCC slab series is 25 and 14 mm higher than N-SCC slab series. It shows that D-SCC slab series are more ductile than N-SCC slab series. The ultimate strength was reached when $P = 53$ kN for D-SCC-a and $P = 52$ kN for D-SCC-b when crushing the top compressive fibre occurred and corresponding deflections were 205 mm and 177 mm.

4.3.3 S-SCC slab series

Slabs S-SCC-a and S-SCC-b containing the 4N12 longitudinal tensile reinforcing bars and PP fibres, with 25 mm clear bottom cover were tested at ages 67 and 69 days respectively. Cracking first occurred approximately at load of $P = 5$ kN in both S-SCC-a and S-SCC-b. The number of cracks increased as the applied load increased and at approximately 70% of the ultimate load, 12 cracks were located inside the high moment region (H.M.R) for S-SCC-a, and 12 cracks for S-SCC-b respectively. The measured final average crack spacings at this load stage were 102 mm for S-SCC-a and 100 mm for S-SCC-b. The ratio of maximum crack width to average crack width at load stage $P = 26$ kN was 1.36 for S-SCC-a and 1.21 for S-SCC-b. The measured maximum and average crack widths within the high moment region at the bottom fibre of the slabs versus applied load are illustrated in Fig. 9.

The measured mid-span deflections of slabs S-SCC-a and S-SCC-b are plotted against load in Fig. 10, respectively. Maximum deflection at failure loading of S-SCC slab series is 25 and 14 mm higher than N-SCC slab series. It shows that S-SCC slab series are more ductile than N-SCC slab series. The ultimate strength was reached when $P = 50$ kN for S-SCC-a and $P = 48$ kN for S-SCC-b when crushing the top compressive fibre occurred and corresponding deflections were 185 mm and 167 mm.

4.3.4 DS-SCC slab series

Slabs DS-SCC-a and DS-SCC-b containing the 4N12 longitudinal tensile reinforcing bars and steel + PP fibres, with 25 mm clear bottom cover were tested at ages 71 and 72 days respectively. Cracking first occurred approximately at load of $P = 8$ kN in both DS-SCC-a and DS-SCC-b. The number of cracks increased as the applied load increased and at approximately 70% of the ultimate load, 13 cracks were located inside the high moment region (H.M.R) for DS-SCC-a, and 12 cracks for DS-SCC-b respectively. The measured final average crack spacings at this load stage were 95 mm for DS-SCC-a and 98 mm for DS-SCC-b. The ratio of maximum crack width to average crack width at load stage $P = 26$ kN was 1.24 for DS-SCC-a and 1.15 for DS-SCC-b. The measured maximum and average crack widths within the high moment region at the bottom fibre of the slabs versus applied load are illustrated in Fig. 11.

The measured mid-span deflections of slabs DS-SCC-a and DS-SCC-b are plotted against load in Fig. 12, respectively. Maximum deflection at failure loading of DS-SCC slab series is 40 and 19 mm higher than N-SCC slab series. It shows that DS-SCC slab series are more ductile than N-SCC slab series. The ultimate strength was reached when $P = 56$ kN for DS-SCC-a and $P = 54$ kN for DS-SCC-b when crushing the top compressive fibre occurred and corresponding deflections were 220 mm and 182 mm.

4.3.5 N-CC slab series (Nejadi 2005)

Slabs N-CC-a and N-CC-b containing the most longitudinal tensile reinforcing bars 4N12, with 25 mm clear bottom cover were tested at ages 62 and 63 days respectively. Cracking first occurred approximately at load of $P = 8$ kN in both N-CC-a and N-CC-b. The number of cracks increased as the applied load increased and at approximately 70% of the ultimate load, 14 cracks were located inside the high moment region for N-CC-a, and 12 cracks for N-CC-b respectively. The measured final average crack spacings at this load stage were 90 mm for N-CC-a and 117 mm for N-CC-b. The ratio of maximum crack width to average crack width at load stage $P = 26$ kN was 1.38 for N-CC-a and 1.28 for N-CC-b. The measured maximum and average crack widths within the high moment region at the bottom fibre of the slabs versus applied load are illustrated in Fig. 13. The crack patterns at approximately 70% of the ultimate load for both slabs are illustrated in Fig. 14. The failure loads were $P = 50$ kN and $P = 47$ kN and corresponding deflections were 136 mm and 156 mm for N-CC-a and N-CC-b, respectively.

5. Discussion on the experimental results

The development and width of flexural cracks in each specimen were carefully monitored under gradually increasing loads up to failure. The first crack appeared in the pure flexure zone within the high moment region. Subsequent cracks appeared with the basic primary crack pattern establishing itself quite rapidly. Secondary cracks appeared between the primary cracks, as the load increased, and a few new cracks occurred at high overload stages. From a comparison of the results it was also observed that crack widths were directly proportional to applied load and consequently to stress in the steel. In addition to the above, the average of all observed crack widths at approximately 70% of the ultimate load was taken and compared with the maximum observed crack width at that load stage. The results are summarised in Table 8. General comparisons of the cracking behaviour test results are summarized as follow:

- Final maximum and average crack widths for N-SCC slab series are slightly more than N-CC slab series and final average spacing of N-SCC-a slab is 5 mm higher than N-CC-a but final average spacing of N-SCC-b slab is 23 mm less than N-CC-b.
- About D-SCC slab series compare to N-SCC and N-CC slab series, final maximum crack widths for D-SCC slab series are slightly less than N-SCC slab series and equal to N-CC slab series. Final average crack widths for D-SCC slab series are less than N-SCC and N-CC slab series. Final average spacing of D-SCC-a slab is 11 mm higher than N-SCC-a and final average spacing of D-SCC-b slab is 2 mm higher than N-SCC-b. Final average spacing of D-SCC-a slab is 16 mm higher than N-CC-a but final average spacing of D-SCC-b slab is 21 mm less than N-CC-b.
- About S-SCC slab series compare to N-SCC and N-CC slab series, final maximum crack widths for S-SCC slab series are slightly less than N-SCC slab series and equal to N-CC slab series. Final average crack widths for S-SCC slab series are less than N-SCC and N-CC slab series. Final average spacing of S-SCC-a slab is 7 mm higher than N-SCC-a and final average spacing of S-SCC-b slab is 6 mm higher than N-SCC-b. Final average spacing of S-SCC-a slab is 12 mm higher than N-CC-a but final average spacing of S-SCC-b slab is 17 mm less than N-CC-b.
- About DS-SCC slab series compare to N-SCC and N-CC slab series, final maximum crack widths for DS-SCC slab series are less than N-SCC and N-CC slab series. Final average crack widths for DS-SCC slab series are less than N-SCC and N-CC slab series. Final average

spacing of DS-SCC-a slab is equal to N-SCC-a and final average spacing of DS-SCC-b slab is 4 mm higher than N-SCC-b. Final average spacing of DS-SCC-a slab is 5 mm higher than N-CC-a but final average spacing of DS-SCC-b slab is 19 mm less than N-CC-b.

6. Short term bond shear stress

The SFRC experimental results included in the database were gathered mainly from papers presented at various published articles. The database includes information regarding the composition of the mixtures, fresh properties of SFRC, testing methodology, and conditions. Thermal characteristics have not been investigated as much as the other aspects of SFRC. The force in the bar is transmitted to the surrounding concrete by bond shear stress τ_b . Due to this transfer, the force in a reinforcing bar changes along its length. The transfer of forces across the interface by bond between concrete and steel is of fundamental importance to many aspects of reinforced concrete behaviour. Under service conditions $\sigma_s < f_{sy}$ and according to Marti *et al.* (1998), $\tau_b = 2 f_{ct}$. To investigate the influence of the assumed bond shear stress on the predicted crack width, five different values for bond shear stress ($\tau_b = f_{ct}$, $\tau_b = 1.5 f_{ct}$, $\tau_b = 2 f_{ct}$, $\tau_b = 3 f_{ct}$, and Eq.(5)) have been considered. For each assumed bond shear stress, the crack widths were calculated and compared with the measured crack widths for each load increment. Instantaneous crack width calculations for concrete reinforced with bars are different from concrete reinforced with bars and fibres, following sections 6.1 and 6.2 described crack width calculations in both conditions.

6.1 Crack width calculations of steel bar reinforcement concrete

Gilbert (2008) proposed a model for predicting the maximum final crack width in reinforced concrete flexural members based on the Tension Chord Model of Marti *et al.* (1998). The model was shown to provide good agreement with the measured final spacing and width of cracks in a range of reinforced concrete beams and slabs tested in the laboratory under sustained service loads for periods in excess of 400 days (Gilbert and Nejadi 2004). Consider a segment of a singly reinforced beam of rectangular section subjected to an in-service bending moment, M_s , greater than the cracking moment, M_{cr} . The spacing between the primary cracks is s . The cracked beam is idealised as a compression chord of depth kd and width b and a cracked tension chord consisting of the tensile reinforcement of area A_{st} surrounded by an area of tensile concrete (A_{ct}). The centroids of A_{st} and A_{ct} are assumed to coincide at a depth d below the top fibre of the section.

For the sections containing a primary crack, $A_{ct} = 0$ and the depth of the compressive zone, kd , and the second moment of area about the centroidal axis (I_{cr}) may be determined from a cracked section analysis using modular ratio theory. Away from the crack, the area of the concrete in the tension chord (A_{ct}) is assumed to carry a uniform tensile stress (σ_{ct}) that develops due to the bond stress (τ_b) that exists between the tensile steel and the surrounding concrete. For the tension chord, the area of concrete between the cracks, A_{ct} , may be taken as:

$$A_{ct} = 0.5(D - kd)b^* \quad (1)$$

where b^* is the width of the section at the level of the centroid of the tensile steel (i.e. at the depth d) but not greater than the number of bars in the tension zone multiplied by $12d_b$.

At each crack, the concrete carries no tension and the tensile steel stress is $\sigma_{st1} = T / A_{st}$, where:

$$T = \frac{n M_s (d - kd)}{I_{cr}} A_{st} \quad (2)$$

$$k = \sqrt{(n\rho)^2 + 2n\rho} - n\rho \quad (3)$$

where ρ is the tensile reinforcement ratio, A_{st} / bd . It should be noted that k (and hence the depth to the neutral axis kd) depends only on the modular ratio n and the reinforcement ratio ρ and is independent of the applied moment M . The depth to the neutral axis remains constant after cracking as the moment increases, until either the concrete compressive stress distribution becomes curvilinear or the reinforcing steel yields.

The second moment of area of the cracked section is:

$$I_{cr} = \frac{1}{2} b d^3 k^2 (1 - k/3) \quad (4)$$

As the distance z from the crack in the direction of the tension chord increases, the stress in the steel reduces due to the bond shear stress τ_b between the steel and the surrounding tensile concrete. For reinforced concrete under service loads, where σ_{st1} is less than the yield stress f_y , Marti *et al.* [28] assumed a rigid-plastic bond shear stress-slip relationship, with $\tau_b = 2.0 f_{ct}$ at all values of slip, where f_{ct} is the direct tensile strength of the concrete. To account for the reduction in bond stress with time due to tensile creep and shrinkage, Gilbert (2008) took the bond stress to be $\tau_b = 2.0 f_{ct}$ for short-term calculations and $\tau_b = 1.0 f_{ct}$ when the final long-term crack width was to be determined. Experimental observations (Gilbert and Nejadi 2004; Wu and Gilbert 2009), indicate that τ_b reduces as the stress in the reinforcement increases and, consequently, the tensile stresses in the concrete between the cracks reduces (i.e. tension stiffening reduces with increasing steel stress). In reality, the magnitude of τ_b is affected by many factors, including steel stress, concrete cover, bar spacing, transverse reinforcement (stirrups), lateral pressure, compaction of the concrete, size of bar deformations, tensile creep and shrinkage. It is recommended here that in situations where the concrete cover and the clear spacing between the bars are greater than the bar diameter, the bond stress τ_b may be taken as:

Table 8 Summary of the results from short-term flexural test

Specimen	Testing age (days)	$(w_{max})_{final}$ (mm)	$(w_{ave})_{final}$ (mm)	$(S_{ave})_{final}$ (mm)	Failure load (kN)	Deflection at failure load (mm)	w_{max} / w_{ave}
N-SCC-a	62	0.20	0.154	95	49.0	180	1.29
N-SCC-b	63	0.25	0.195	94	48.5	163	1.17
D-SCC-a	65	0.18	0.138	106	53.0	205	1.10
D-SCC-b	66	0.23	0.172	96	52.0	177	1.33
S-SCC-a	67	0.18	0.132	102	50.0	185	1.36
S-SCC-b	69	0.23	0.189	100	48.0	167	1.21
DS-SCC-a	71	0.15	0.120	95	56.0	220	1.24
DS-SCC-b	72	0.20	0.156	98	54.0	182	1.15
N-CC-a	62	0.18	0.130	90	50.0	136	1.38
N-CC-b	63	0.23	0.180	117	47.0	156	1.28

$$\tau_b = \lambda_1 \lambda_2 \lambda_3 f_{ct} \quad (5)$$

where λ_1 accounts for the load duration with $\lambda_1 = 1.0$ for short-term calculations and $\lambda_1 = 0.7$ for long-term calculations; λ_2 is a factor that accounts for the reduction in bond stress as the steel stress σ_{st1} increases and is given by (Wu and Gilbert, 2009):

$$\lambda_2 = 1.66 - 0.003 \sigma_{st1} \geq 0.0 \quad (6)$$

and λ_3 is a factor that accounts for the very significant increase in bond stress that has been observed in laboratory tests for small diameter bars (Gilbert and Nejadi 2004) and may be taken as:

$$\lambda_3 = 7.0 - 0.3 d_b \geq 2.0 \quad (7)$$

Following the approach of Marti *et al.* (1998), the concrete and steel tensile stresses, where $0 < z \leq s/2$, may be expressed as:

$$\sigma_{sz} = \frac{T}{A_{st}} - \frac{4 \tau_b z}{d_b} \quad (8)$$

$$\sigma_{cz} = \frac{4 \tau_b \rho_{tc} z}{d_b} \quad (9)$$

where ρ_{tc} is the reinforcement ratio of the tension chord ($= A_{st}/A_{ct}$) and d_b is the reinforcing bar diameter. Mid-way between the cracks, at $z = s/2$, the stresses are:

$$\sigma_{st2} = \frac{T}{A_{st}} - \frac{2 \tau_b s}{d_b} \quad (10)$$

$$\sigma_{c2} = \frac{2 \tau_b \rho_{tc} s}{d_b} \quad (11)$$

The maximum crack spacing immediately after loading, $s = s_{max}$, occurs when $\sigma_{c2} = f_{ct}$, and from Eq. (11):

$$s_{max} = \frac{f_{ct} d_b}{2 \tau_b \rho_{tc}} \quad (12)$$

with $\lambda_1 = 1.0$ in Eq. (5). If the spacing between two adjacent cracks just exceeds s_{max} , the concrete stress mid-way between the cracks will exceed f_{ct} and another crack will form between the two existing cracks. It follows that the minimum crack spacing is half the maximum value, that is, $s_{min} = s_{max}/2$.

The short term crack width $(w_i)_{tc}$ in the fictitious tension chord is the difference between the elongation of the tensile steel over the length s and the elongation of the concrete between the cracks and is given by:

$$(w_i)_{tc} = \frac{s}{E_s} \left[\frac{T}{A_{st}} - \frac{\tau_b s}{d_b} (1 + n\rho_{tc}) \right] \quad (13)$$

6.2 Crack width calculations of steel bar reinforcement concrete with fibres

Leutbecher and Fehling (2008) have derived a cracking behaviour model based on the assumptions of constant bond stress and a parabolic development of concrete and steel strains between the cracks. To calculate crack widths, the assumption of parabolic strain development is used to determine a mean steel strain and a mean concrete strain. The maximum crack width is calculated as twice the transfer length multiplied by the difference between the concrete and steel mean strains:

$$w_{max} = 2l_{es} (\varepsilon_{sm} - \varepsilon_{cm}) \quad (14)$$

where w_{max} is the maximum crack width, mm; l_{es} is the transfer length, mm; ε_{sm} is the mean steel strain; ε_{cm} is the mean concrete strain.

The above equation can be re-written for the initial crack as:

$$w_{max} = \frac{(\sigma_{cf,cr}^i - \sigma_{cf}) d_b}{5 E_s \tau_{sm} \rho_s^2} \left[(1 + \alpha_E \rho_s) \sigma_{cf,cr}^i - \sigma_{cf} \right] \quad (15)$$

where σ_{cf} is the stress in the fibre reinforced concrete; $\sigma_{cf,cr}^i$ is the imaginary cracking stress of the fibre reinforced concrete; τ_{sm} is the average bond stress over load transmission length; d_b is the reinforcing bar diameter, mm; E_s is the modulus of elasticity of reinforcing bar; ρ_s is the reinforcing ratio of steel reinforcement; α_b is the shape coefficient of strain courses ($\alpha_b = 0.6$ for short term loading, $\alpha_b = 0.4$ for long term or repeated loading), α_E is the ratio of the modulus of elasticity of steel to the modulus of elasticity of concrete, $\alpha_E = E_s/E_c$.

A similar equation can be used for stabilized cracking:

$$w_{max} = \frac{(\sigma_{cf,cr}^i - \sigma_{cf}) d_b}{5 E_s \tau_{sm} \rho_s^2} \left[\sigma_s - 0.6 \frac{\sigma_{cf,cr}^i}{\rho_s} (1 + \alpha_E \rho_s) \sigma_{cf,cr}^i - 0.6 \frac{\sigma_{cf}}{\rho_s} \right] \quad (16)$$

where σ_s is the stress in the reinforcing bar at a crack. This can be calculated from the following equation:

$$\sigma_s = \frac{F}{A_s} - \frac{\sigma_{cf}}{\rho_s} \quad (17)$$

where F is the applied load; A_s is the cross-sectional area of the steel bars.

The maximum crack spacing during the progressive cracking phase can also be determined, using the following equation:

$$s_{r,max} = (\sigma_{cf,cr}^i - \sigma_{cf0}) \frac{d_b}{2 \tau_{sm} \rho_s} \quad (18)$$

where $s_{r,max}$ is the maximum crack spacing.

$$\sigma_{cf} = f_{ct} \left(1 - \frac{w f_{ct}}{2 G_f} \right) + \sigma_{cf0} \left(2 \sqrt{\frac{w}{w_0}} - \frac{w}{w_0} \right) \quad (19)$$

where w is the crack width; f_{ct} is the concrete matrix tensile strength; G_f is the fracture energy of the concrete matrix; σ_{cf0} is the maximum post-cracking stress; w_0 is the crack width corresponding to maximum post-cracking stress.

During the fibre pullout phase, the fibre stress can be calculated from the following equation:

$$\sigma_{cf} = \sigma_{cf0} \left(1 - \frac{w}{l_f} \right) \quad (20)$$

where σ_{cf0} is the maximum post-cracking stress and for fibres with a random orientation, it can be calculated as:

$$\sigma_{cf0} = \eta g \rho_f \frac{\tau_{fm} l_f}{d_f} \quad (21)$$

where η is the coefficient of fibre orientation; g is the coefficient of fibre efficiency (i.e., – damage factor); ρ_f is the volume fraction of fibres; l_f is the fibre length; d_f is the fibre diameter, mm; τ_{fm} is the mean fibre-matrix bond stress. The mean fibre-matrix bond stress can be approximated as:

$$\tau_{fm} = 1.3 f_{ctm} \quad (22)$$

where f_{ctm} is the mean tensile strength of the plain concrete matrix.

The fibre orientation and efficiency coefficients, η and g , are more difficult to define and must be determined experimentally. σ_{cf0} can easily be determined from direct tension tests, and the coefficient of fibre efficiency can be determined from these as follows:

$$g = \frac{\sigma_{cf0} d_f}{\eta \rho_f \tau_{fm} l_f} \quad (23)$$

However, the fibre orientation coefficient, η , must be derived from a large number of tests for a variety of fibre types. More study is required to create an adequate formulation. As stated above, w_0 is the crack width corresponding to σ_{cf0} , the maximum post-cracking stress. It can be calculated from the following equation:

$$w_0 = \frac{\tau_{fm} l_f^2}{E_f d_f} \quad (24)$$

where E_f is the modulus of elasticity of the fibres.

The imaginary cracking stress, $\sigma_{cf,cr}^i$ is the maximum stress of the ascending fibre phase. It can be calculated by substituting the crack width corresponding to the maximum stress of the ascending fibre activation phase into the equation for the fibre reinforced concrete stress:

$$w^* = \frac{w_0}{\left(1 + \frac{w_0 f_{ct}^2 g}{2 \sigma_{cf0} G_f}\right)} \quad (25)$$

This equation was determined by taking the derivative of σ_{cf} and setting it to zero. The imaginary cracking stress is then calculated using the following equation:

$$\sigma_{cf,cr}^i = f_{ct} \left(1 - \frac{w^* f_{ct}}{2 G_f}\right) + \sigma_{cf0} \left(2 \sqrt{\frac{w^*}{w_0}} - \frac{w^*}{w_0}\right) \quad (26)$$

Eq. (13) is used for N-SCC slab series crack width calculations and Eq.(16) is used for D-SCC, S-SCC, and DS-SCC slab series crack width calculations. The results are presented in Tables 9-12. Measured and calculated maximum crack widths versus steel stress and different bond shear stresses are illustrated in Figs. 15-18. Also, the results of Nejadi (2005) are presented for comparison with SCC slab series in Fig. 19 and Table 13.

The comparisons show that the proposed bond shear stress for CC (Eq.(5)) is not suitable for SCC slab series. Also, the calculated crack width by using the CC bond shear stress is underestimated for all of SCC slab series. As Figs. 15-19 show $\tau_b = f_{ct}$ is made crack width calculation overestimated for all SCC slab series. The crack width calculation is underestimated by using $\tau_b = 2 f_{ct}$ and $\tau_b = 3 f_{ct}$ bond shear stresses (see Figs. 15-19). About $\tau_b = 1.5 f_{ct}$ bond shear stress is roughly suitable for most of the SCC slab series but it is not the adopted bond shear stress in this study for the SCC slabs because it makes crack calculation underestimating for D-SCC slab series and overestimating for N-CC slab series (see Figs. 15-19).

6.3 Adopted bond shear stress for crack width calculation of SCC slabs

Five different values for bond shear stress ($\tau_b = f_{ct}$, $\tau_b = 1.5 f_{ct}$, $\tau_b = 2 f_{ct}$, $\tau_b = 3 f_{ct}$, and Eq.(5)) have been considered and the corresponding crack widths were calculated and compared with the experimental results for each load increment. It should be mentioned that throughout the test, crack widths were monitored at two levels on the side of each specimens, i.e., the steel level and bottom fibre. In general, cracking in reinforced concrete is a random phenomenon with every experimental result subjected to both systematic and random errors. For example, repeated measurements of the crack widths during each load increment differed, even when the measurements were performed by the same microscope, under the same conditions. The measurements varied according to the exact location of the measurement on the crack, as the crack side faces are irregular and not parallel. Considering this and comparing the best fit between the calculated values and measured crack widths, the expressions for the bond shear stress τ_b for SCC slab series are presented in Table 14 and Fig. 20, under short-term loading and for the different in-service steel stress ranges have been adopted for the analytical model.

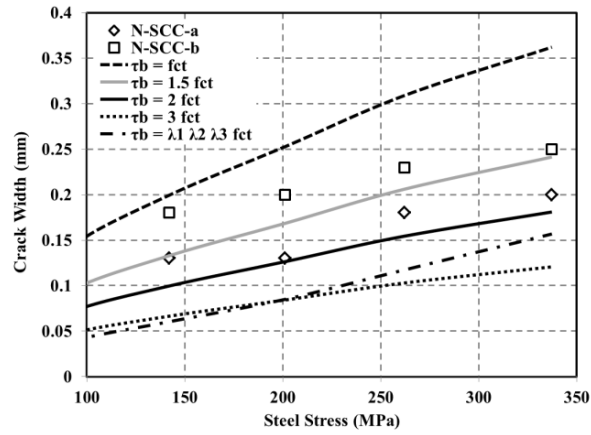


Fig. 15 Comparison of different bond stresses for slab N-SCC series

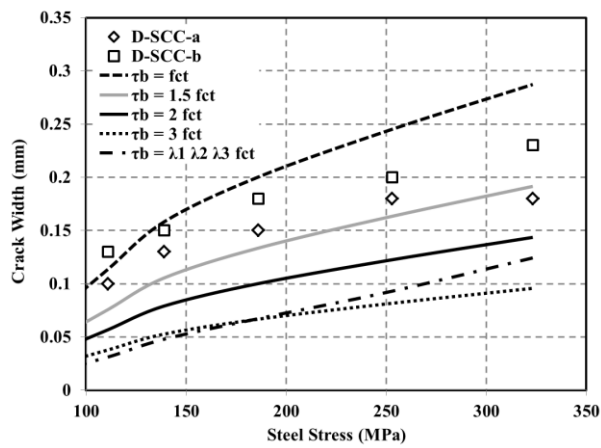


Fig. 16 Comparison of different bond stresses for slab D-SCC series

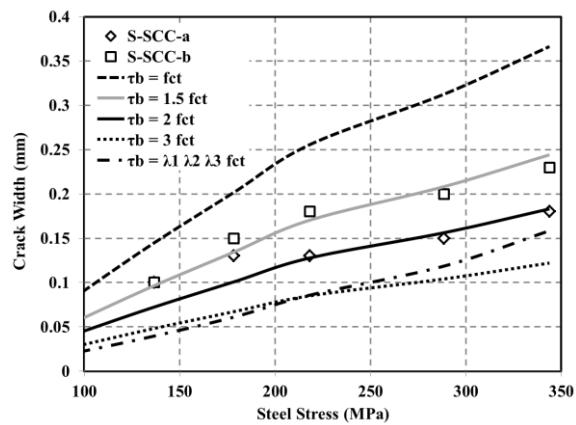


Fig. 17 Comparison of different bond stresses for slab S-SCC series

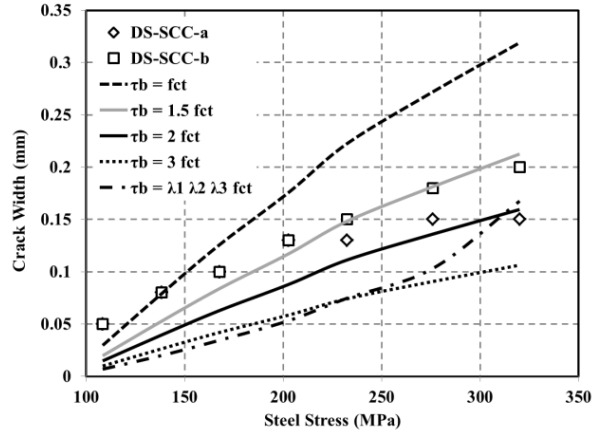


Fig. 18 Comparison of different bond stresses for slab DS-SCC series

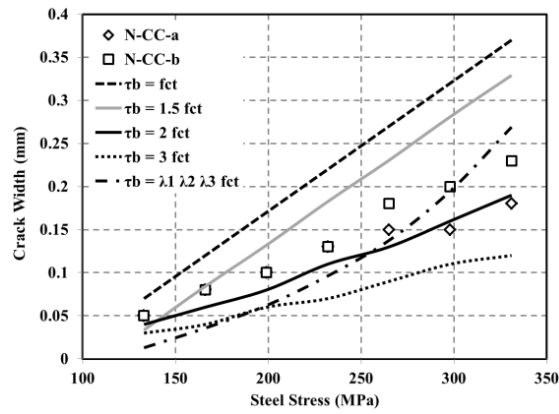


Fig. 19 Comparison of different bond stresses for slab DS-SCC series

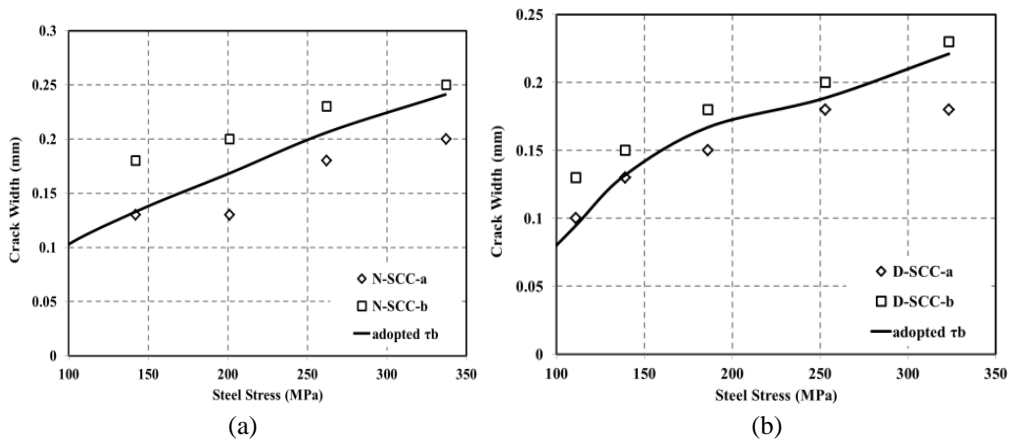


Fig. 20 Adopted bond stresses for (a) N-SCC, (b) D-SCC, (c) S-SCC, and (d) DS-SCC slab series

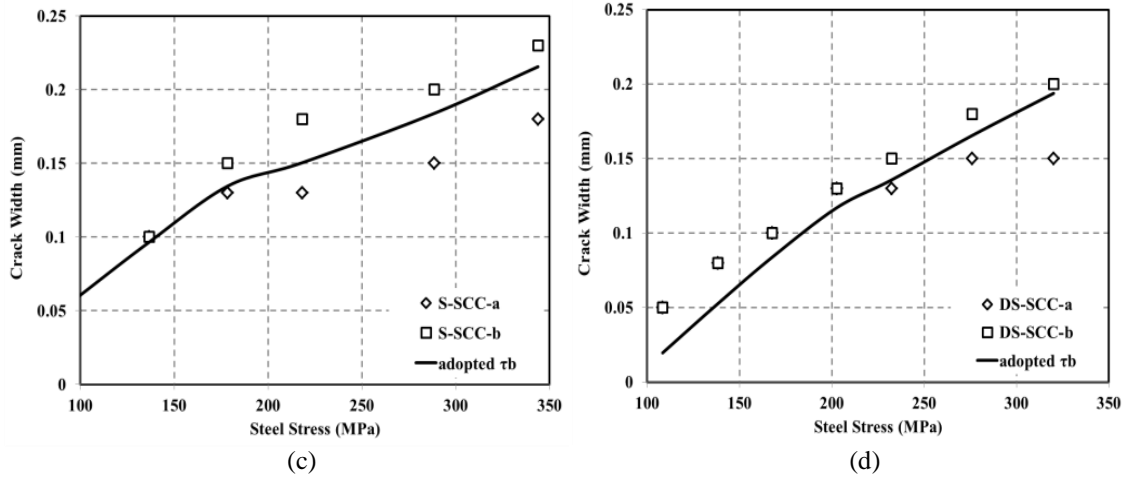


Fig. 20 Continued

Table 9 Measured and calculated maximum crack width for slab N-SCC series

(N-SCC)	M (kNm)	σ_{st} (MPa)	Maximum crack width (mm)						
			Measured		Calculated				
			N-SCC-a	N-SCC-b	$\tau_b = f_{ct}$	$\tau_b = 1.5 f_{ct}$	$\tau_b = 2 f_{ct}$	$\tau_b = 3 f_{ct}$	$\tau_b = \lambda_1 \lambda_2 \lambda_3 f_{ct}$
	7.00	60	0.05	0.08	0.034	0.022	0.017	0.011	0.008
	8.80	84	0.08	0.13	0.090	0.060	0.045	0.030	0.022
	10.5	93	0.10	0.15	0.143	0.095	0.072	0.048	0.039
	12.3	142	0.13	0.18	0.199	0.133	0.099	0.066	0.060
	14.0	201	0.13	0.20	0.252	0.168	0.126	0.084	0.085
	15.8	262	0.18	0.23	0.309	0.206	0.154	0.103	0.117
	17.5	337	0.20	0.25	0.362	0.241	0.181	0.121	0.157

Table 10 Measured and calculated maximum crack width for slab D-SCC series

(D-SCC)	M (kNm)	σ_{st} (MPa)	Maximum crack width (mm)						
			Measured		Calculated				
			D-SCC-a	D-SCC-b	$\tau_b = f_{ct}$	$\tau_b = 1.5 f_{ct}$	$\tau_b = 2 f_{ct}$	$\tau_b = 3 f_{ct}$	$\tau_b = \lambda_1 \lambda_2 \lambda_3 f_{ct}$
	7.00	60	0.05	0.05	0.027	0.018	0.013	0.009	0.006
	8.80	85	0.08	0.08	0.071	0.047	0.036	0.024	0.018
	10.5	111	0.10	0.13	0.113	0.075	0.057	0.038	0.032
	12.3	139	0.13	0.15	0.158	0.105	0.079	0.053	0.048
	14.0	186	0.15	0.18	0.200	0.133	0.100	0.067	0.067
	15.8	253	0.18	0.20	0.245	0.163	0.122	0.082	0.093
	17.5	323	0.18	0.23	0.287	0.191	0.143	0.096	0.124

Table 11 Measured and calculated maximum crack width for slab S-SCC series

(S-SCC)		Maximum crack width (mm)						
M (kNm)	σ_{st} (MPa)	Measured		Calculated				
		S-SCC-a	S-SCC-b	$\tau_b = f_{ct}$	$\tau_b = 1.5 f_{ct}$	$\tau_b = 2 f_{ct}$	$\tau_b = 3 f_{ct}$	$\tau_b = \lambda_1 \lambda_2 \lambda_3 f_{ct}$
7.00	62	0.05	0.08	0.034	0.022	0.017	0.011	0.008
8.80	100	0.08	0.08	0.091	0.060	0.045	0.030	0.023
10.5	137	0.10	0.10	0.145	0.096	0.072	0.048	0.040
12.3	178	0.13	0.15	0.202	0.134	0.101	0.067	0.061
14.0	218	0.13	0.18	0.255	0.170	0.128	0.085	0.085
15.8	289	0.15	0.20	0.312	0.208	0.156	0.104	0.118
17.5	344	0.18	0.23	0.366	0.244	0.183	0.122	0.158

Table 12 Measured and calculated maximum crack width for slab DS-SCC series

(DS-SCC)		Maximum crack width (mm)						
M (kNm)	σ_{st} (MPa)	Measured		Calculated				
		DS-SCC-a	DS-SCC-b	$\tau_b = f_{ct}$	$\tau_b = 1.5 f_{ct}$	$\tau_b = 2 f_{ct}$	$\tau_b = 3 f_{ct}$	$\tau_b = \lambda_1 \lambda_2 \lambda_3 f_{ct}$
7.00	108	0.05	0.05	0.029	0.020	0.015	0.010	0.007
8.80	138	0.08	0.08	0.079	0.053	0.039	0.026	0.020
10.5	168	0.10	0.10	0.126	0.084	0.063	0.042	0.034
12.3	203	0.13	0.13	0.176	0.117	0.088	0.058	0.053
14.0	232	0.13	0.15	0.222	0.148	0.111	0.074	0.074
15.8	276	0.15	0.18	0.272	0.181	0.136	0.090	0.103
17.5	320	0.15	0.20	0.319	0.212	0.159	0.106	0.167

Table 13 Measured and calculated maximum crack width for slab N-CC series

(N-CC)		Maximum crack width (mm)						
M (kNm)	σ_{st} (MPa)	Measured		Calculated				
		N-CC-a	N-CC-b	$\tau_b = f_{ct}$	$\tau_b = 1.5 f_{ct}$	$\tau_b = 2 f_{ct}$	$\tau_b = 3 f_{ct}$	$\tau_b = \lambda_1 \lambda_2 \lambda_3 f_{ct}$
7.00	133	0.05	0.05	0.070	0.033	0.040	0.030	0.013
8.80	166	0.08	0.08	0.120	0.084	0.060	0.040	0.036
10.5	199	0.10	0.10	0.170	0.132	0.080	0.060	0.062
12.3	232	0.13	0.13	0.220	0.182	0.110	0.070	0.096
14.0	265	0.15	0.18	0.270	0.230	0.130	0.090	0.138
15.8	298	0.15	0.20	0.320	0.281	0.160	0.110	0.195
17.5	331	0.18	0.23	0.370	0.329	0.190	0.120	0.269

Table 14 Adopted bond shear stresses for SCC slab series

Slab series	τ_b	
	$f_{sv} > \sigma_{s,max} \geq 180$ MPa	$\sigma_{s,max} < 180$ MPa
N-SCC	$1.50 f_{ct}$	$1.50 f_{ct}$
D-SCC	$1.30 f_{ct}$	$1.25 f_{ct}$
S-SCC	$1.70 f_{ct}$	$1.50 f_{ct}$
DS-SCC	$1.60 f_{ct}$	$1.50 f_{ct}$

7. Conclusions

The following conclusions can be drawn from this experimental study:

1. The DS-SCC slab series are shown the lowest maximum and average final crack widths compare to the other mixtures slab series. The DS-SCC slab series are bearded maximum failure load and deflection compare to the other mixtures slab series.

2. The S-SCC slab series are decreased maximum and average final crack widths compared to N-SCC slab series but not much changed compared to N-CC slab series. Using PP fibres in SCC did not change failure loading much but it is increased the ductility of slab specimens compared to N-SCC and N-CC slab series.

3. Using steel fibres in SCC are decreased maximum and average final crack widths compare to N-SCC and N-CC slab series. The D-SCC slab series are decreased final average spacings compared to the other mixtures slab series.

4. The $\tau_b = 1.5 f_{ct}$ bond shear stress is roughly suitable for most of the SCC slab series but it is not the adopted bond shear stress in this study for the SCC slabs because it makes crack calculation underestimating for D-SCC slab series and overestimating for N-CC slab series.

5. The crack widths calculated by using adopted bond shear stresses for SCC and FRSCC slabs are in good agreement with experimental results.

Acknowledgements

This work was supported by Centre for Built Infrastructure Research, School of Civil and Environmental Engineering, University of Technology Sydney, Australia. The authors would like to express their sincere gratitude and appreciation to Boral, BOSFA, and Concrete companies.

References

- ACI 232.2R-03 (2004), "Use of Fly Ash in Concrete", ACI Committee 232.
- ACI 233R-95 (2000), "Ground granulated blast-furnace slag as a cementitious constituent in concrete," ACI Committee 233.
- ACI 237R-07 (2007), "Self-consolidating concrete", ACI Committee 237.
- ACI 544.2R (1999), *State-of-the-Art Report on Fiber Reinforced Concrete*, Technical report, American Concrete Institute.
- AS 1012.10 (2000), "Determination of indirect tensile strength of concrete cylinders".
- AS 1012.11 (2000), "Determination of modulus of rupture".
- AS 1012.14 (1991), "Method for securing and testing from hardened concrete for compressive strength".
- AS 1012.17 (1997), "Determination of the static chord modulus of elasticity and Poisson's ratio of concrete specimens".
- AS 1141 (2011), "Methods for sampling and testing aggregates - particle size distribution - sieving method", Standards Australia.
- AS 1478.1 (2000), "Chemical admixtures for concrete, mortar and grout - Admixtures for concrete", Standards Australia.
- AS 2350 (2006), "Methods of testing portland and blended cements", Standards Australia.

- AS 3582.2 (2001), "Supplementary cementitious materials for use with portland and blended cement - Slag - Ground granulated iron blast-furnace", Standards Australia.
- AS 3583 (1998), "Methods of test for supplementary cementitious materials for use with portland cement", Standards Australia.
- AS 3972 (2010), "General purpose and blended cements", Standards Australia.
- Aslani, F. and Nejadi, S. (2012a), "Mechanical properties of conventional and self-compacting concrete: An analytical study", *Constr. Build. Mater.*, **36**, 330-347.
- Aslani, F. and Nejadi, S. (2012b), "Bond characteristics of steel fibre reinforced self-compacting concrete", *Can. J. Civil Eng.*, **39**(7), 834-848.
- Aslani, F. and Nejadi, S. (2012c), "Bond behavior of reinforcement in conventional and self-compacting concrete," *Adv Struct Eng*, **15**(12), 2033-2051.
- Aslani, F. and Nejadi, S. (2013a), "Self-compacting concrete incorporating steel and polypropylene fibers: compressive and tensile strengths, moduli of elasticity and rupture, compressive stress-strain curve, and energy dissipated under compression", *Compos Part B-Eng*, **53**, 121-133.
- Aslani, F. and Nejadi, S. (2013b), "Creep and shrinkage of self-compacting concrete with and without fibers", *J. Adv. Concr. Technol.*, **11**(10), 251-265.
- Aslani, F. (2013), "Effects of specimen size and shape on compressive and tensile strengths of self-compacting concrete with or without fibers", *Mag Concrete Res*, **65**(15), 914-929.
- Aslani, F. and Natoori, M. (2013), "Stress-strain relationships for steel fibre reinforced self-compacting concrete", *Struct. Eng. Mech.*, **46**(2), 295-322.
- ASTM standards (2000), Volume 04.02, "Concrete and aggregates".
- ASTM C183-08 (2000), "Standard practice for sampling and the amount of testing of hydraulic cement," ASTM standards 2000 (Annual book).
- ASTM C31 -11b (2000), "Standard test methods for sampling and testing fly ash or natural pozzolans for use in portland-cement concrete," ASTM standards 2000 (Annual book), 2000.
- ASTM C989-06 (2000), "Standard specification for ground granulated blast-furnace slag for use in concrete and mortars," ASTM standards 2000 (Annual book).
- ASTM C1077-13 (2000), "Standard Practice for Agencies Testing Concrete and Concrete Aggregates for Use in Construction and Criteria for Testing Agency Evaluation", ASTM standards 2000.
- Deutscher Beton-Verein EV, DBV-Merkblatt. Bemessungsgrundlagen für Stahlfaserbeton im Tunnelbau, Eigenverlag; 1996.
- European guidelines (2005), "The european guidelines for self-compacting concrete, Specification, production and use".
- Gilbert, R.I. (2008), "Control of flexural cracking in reinforced concrete", *ACI Struct. J*, 105(3), 301-307.
- Gilbert, R.I. and Nejadi, S. (2004), *An Experimental Study of Flexural Cracking in Reinforced Concrete Members under Sustained Loads*, UNICIV Report No. R-435, School of Civil and Environmental Engineering, University of New South Wales, Sydney, Australia.
- Kooiman, A.G. (2000), "Modelling steel fibre reinforced concrete for structural design", Dissertation, Technische Universiteit Delft.
- Leutbecher, T. and Fehling, E. (2008), "Crack Formation and Tensile Behaviour of UHPC Reinforced with a Combination of Rebars and Fibres", In: Schmidt, M., Fehling, E., Stürwald, S. (Eds.) *Ultra High Performance Concrete (UHPC)*, Second International Symposium on Ultra High Performance Concrete. *Struct. Mater. Eng. Series*, **10**, 497-504.
- Maia, L., Azenha, M., Geiker, M. and Figueiras, J. (2012), "E-modulus evolution and its relation to solids formation of pastes from commercial cements", *Cem. Concr. Res.*, **42**, 928-936.
- Marti, P., Alvarez, M., Kaufmann, W. and Sigrist, V. (1998), "Tension chord model for structural concrete," *Struct. Eng. Int.*, **4**, 287-298.
- Nejadi, S. (2005), "Time-dependent cracking and crack control in reinforced concrete structures", Ph.D. Thesis, The University of New South Wales.
- RILEM TC 162-TDF (2002), "Test and design methods for steel fibre reinforced concrete", Final recommendations, *Mater. Struct.*, **35**, 579-582.

RTA (Regional Transportation Authority) (2006), "Materials test methods", **1**.

Wu, H.Q. and Gilbert, R.I. (2009), "Modelling short-term tension stiffening in reinforced concrete prisms using a continuum-based finite element model", *Eng. Struct.*, **31**(10), 2380-2391.

CC